

Multi-focus Image Fusion Based on Image Decomposition and Quad Tree Decomposition

Yongxin Zhang^{1,2} Li Chen¹ Zihua Zhao¹ Jian Jia³

¹ School of Information Science and Technology, Northwest University,

Xi'an, 710127, China

chenli@nwu.edu.cn

² Luoyang Normal University,

Luoyang, 471022, China,

tabo126@126.com

³ Department of Mathematics, Northwest University,

Xi'an, 710127, China

jiajian@nwu.edu.cn

Received 7 January 2014; Revised 30 April 2014; Accepted 17 June 2014

Abstract. In order to efficiently represent source images and inhibit the blocking artifacts, a novel multi-focus image fusion scheme based on image decomposition and quad tree (QT) decomposition is proposed. The registered source images are first decomposed into cartoon and texture components by using image decomposition, and then, QT decomposition is performed on the cartoon and texture components. The salient features of the cartoon and texture components construct the feature space. The focused regions of the source images are detected by the salient features of the cartoon and texture components. The final fused image can be produced by combining the image regions that corresponding to the focused component regions. Experimental results have demonstrated that the proposed method can efficiently inhibit the blocking artifacts and significantly improve the fusion quality compared to the other existing fusion methods in both spatial and transform domain.

Keywords: image fusion, image decomposition, quad tree decomposition, total variation

1 Introduction

Multi-focus image fusion can be defined as the process of combing substantial information from multiple images of the same scene to create a single composite image that will be more suitable for human visual perception or further computer processing [1]. It has been proven to be an effective way to extend the depth of the field [2]. In general, the image fusion methods can be categorized into two groups: spatial domain fusion and transform domain fusion [3]. In this paper, we concentrate on spatial domain methods.

The spatial domain fusion methods can be divided into two categories: pixel based methods and region based methods. In spatial domain, the simplest pixel based fusion method is to take the average of the source images pixel by pixel. However, the simplicity may reduce the contrast of the fused image. To improve the quality of the fused image, some region based methods have been proposed to combine the partitioned blocks or segmented regions based on their sharpness [4]. The sharpness is measured by the local spatial features [5] such as energy of image gradient (EOG) and spatial frequency (SF) [4]. Then, the focused blocks or regions are selected from source images by being simply copied into the fused image. However, if the size of the blocks is too small, the block selection is sensitive to noise and subject to incorrect selection of blocks from the corresponding source images. Or else, if too large, the in-focus and out-of-focus pixels are partitioned in the same block, which is selected to build the final fused image. Accordingly, the blocking artifacts are produced and may compromise the quality of the final fused image. To eliminate the blocking artifacts, researchers have proposed some improved schemes. Goshtasby et al. [6] have detected the focused blocks by computing the weight sum of the blocks and significantly eliminated the blocking artifacts. But the iterative procedure is time-consuming. Huang et al. [7] have detected the focused blocks by using pulse-coupled neural networks (PCNN) and improved the visual quality of the fused image. But the parameters of the PCNN are complicated and lack adaptability. Aslantas et al. [8] have selected the block-size by using differential evolution algorithm and enhanced the adaptability of the fusion method. But this method requires longer computational time. De et al. [9] have selected the optimal size of the block division by using quad tree (QT) structure and effectively solved the problem of determining of block size. Wan et al. [10] have selected the focused pixels from the source images by using robust components analysis (RPCA) and obtained better fusion quality. But the RPCA decomposition is time consum-

ing. These schemes all achieve better performance than the traditional methods and significantly inhibit the blocking artifacts.

Image decomposition is an important way of image processing, which separates a given image into cartoon and texture components. The cartoon component holds the geometric structures, isophotes and smooth-piece of source images, while the texture component contains textures, oscillating patterns, fine details and noise [11]. The cartoon and texture components represent the most meaningful information of source images, which are important for image fusion. Image decomposition has been proven to be an effective way to extract the structure information and texture information from image [12]. The objective of this paper is to investigate its potential application in the multi-focus image fusion. The main contribution of this paper is that a multi-focus image fusion framework based on image decomposition and QT decomposition is established. The framework is based on the discriminative features that computed from the cartoon and texture components of the source images. To eliminate the blocking artifacts, the optimal block division is determined by quad tree decomposition. The proposed method can significantly inhibit the blocking artifacts and better represent the source images.

The rest of the paper is organized as follows. In section 2, the basic idea of image decomposition and QT decomposition will be briefly described, followed by the new method based on image decomposition and QT decomposition for image fusion in section 3. In section 4, extensive simulations are performed to evaluate the performance of the proposed method. In addition, several experimental results are presented and discussed. Finally, concluding remarks are drawn in section 5.

2 Related Work

2.1 Image Decomposition

Nowadays, an observed image f represents a real scene in many problems of image analysis [13]. The image f may contain texture or noise. In order to extract the most meaningful information from f , most models [14-23] try to find another image u , "close" to f , such that u is a cartoon or simplification of f . These models assume that there is a relation between the following relation between f and u as follows:

$$f = u + v. \quad (1)$$

where v is noise or texture. In 1989, Mumford et al. [14] have established a model to decompose the black and white static image by using bounded variation function, which is called Mumford-Shah energy functional:

$$E_{MS}(u, C) = \iint_{R \setminus C} (\|\nabla u\|^2 + \lambda(u - u_0)) dx dy + \mu Len(C). \quad (2)$$

where C is the segmenting contour, $\lambda > 0$ and $\mu > 0$ are the weight coefficients. u_0 is the feature of the original image. u is the optimal piecewise approximation of u_0 . In 1992, Rudin et al. [15] have simplified the Mumford-Shah model and proposed total variation minimization energy functional model of Rudin-Osher-Fatemi (ROF) as:

$$E_{ROF}(u) = \iint_R (\|\nabla u\| dx dy + \lambda \iint_R (u - u_0)^2 dx dy). \quad (3)$$

where $\lambda > 0$ is the weight coefficient. The ROF model is efficient for de-noising images while keeping sharp edges. In fact, both Mumford-Shah model and ROF model can minimize the energy function that they have constructed and obtain the correct decomposition of the source image. But Meyer [16] has proved that the ROF model will remove the texture when λ is small enough. In addition, he has introduced the use of a space of functions, which is the dual of the BV space in some sense. In 2002, Vese et al. [17] have combined the total variation minimization in image restoration of ROF model with the ideas introduced by Meyer to model texture or noise. The model is described as:

$$E_{VO}(u, \bar{g}) = \iint_R (\|\nabla u\| dx dy + \lambda \iint_R |u_0 - (u + div(\bar{g}))|^2 dx dy + \mu \|\bar{g}\|_{L^p}). \quad (4)$$

Vese et al. have developed a partial differential equation (PDE) based on iterative numerical algorithm to approximate Meyer's weaker norm $\|\cdot\|_G$ by using L^p . However, this model is time consuming. To improve the computation efficiency, many models and methods have been proposed. Vese et al. have also proposed Osher-

Sole-Vese (OSV) [18] model based on total variation (TV) and norm H^{-1} . Aujol et al. [19] have introduced dual norm to image decomposition. Chana et al [20] have proposed $CEP-H^{-1}$ model based on OSV. However, these models are still complicated. In 2008, Goldstein et al. [21] have proposed Split Bregman algorithm by combining the split method [22] with Bregman iteration [23]. This algorithm is easy to implement and has low computational complexity. This paper performs the image decomposition on the source images based on ROF model by using Split Bregman algorithm.

Fig. 1 shows the decomposition results of source image ‘Clock’. It is obvious that the salient features of the cartoon and texture components of the source image are corresponding to the local features of the objects in focus. Thus, the cartoon and texture components can be used to build a robust fusion scheme to discriminate the focused regions from defocused regions. In this paper, both cartoon and texture components are used to detect the focused blocks.

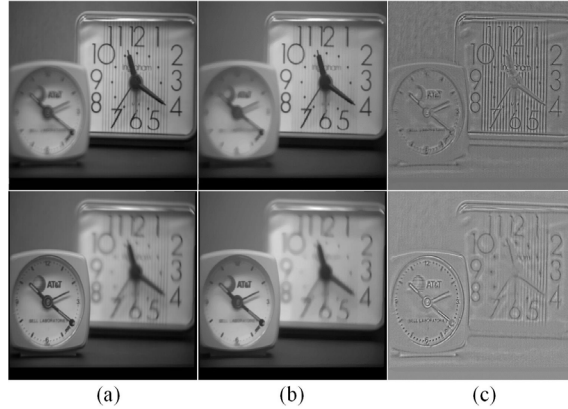


Fig. 1. Decomposition results of multi-focus image ‘Clock’ using image decomposition. (a) Source images I , (b) Cartoon component U , (c) Texture component V .

2.2 Quad Tree Decomposition

QT is an important data structure where each internal node in the tree has exactly four children and each leaf node in the tree has no children. QT decomposition is an analysis technique which can partition an image into blocks that are more homogeneous than the image itself. In traditional QT decomposition, a square image can be partitioned into four equal sized blocks and then each block is evaluated by some threshold conditions of region homogeneity. The block that meets the threshold conditions will not be subdivided further, while the block that doesn’t meet the threshold conditions will be subdivided into four blocks. And then the blocks are evaluated again iteratively until each block meets the threshold conditions [9, 24]. An example of the subdivision of an image in a QT structure is depicted in Fig. 2 (a). The whole image is represented by a root node which is split into four blocks when its homogeneity doesn’t meet the threshold conditions. The image block whose homogeneity meets the threshold conditions is represented by leaf node. In Fig. 2 (a), I_0 is the image at level 0. After initial subdivision, $I_k (k = 1, \dots, 4)$ are corresponding to regions at level 1. At level 1, the first and the third blocks, namely I_1 and I_3 , are subdivided into smaller blocks I_{1k} and $I_{3k} (k = 1, \dots, 4)$ at level 2. According to the rule of QT decomposition, I_{1k} and I_{3k} are further subdivided if they meet the threshold conditions. Other quadrants will be subdivided similarly.

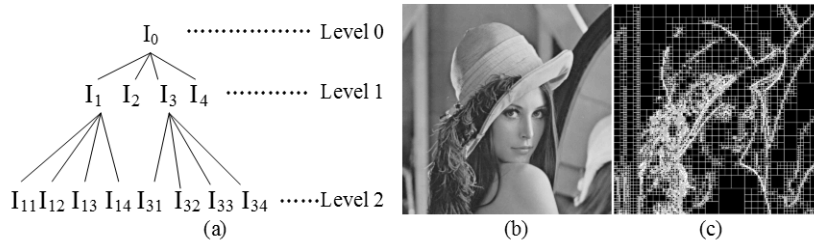


Fig. 2. QT decomposition of an image. (a) Subdivision of an image into quad tree structure, (b) Source image ‘Lena’, (c) QT decomposition result of ‘Lena’.

It has been proved that the QT decomposition has the advantages of self-adaptation and high speed [24]. It is obvious that the salient features such as edges and textures of Fig. 2 (c) are corresponding to the salient feature of Fig. 2 (b). One can see that the block size of the subdivision in Fig. 2 (c) is changing with the region homogeneity of Fig. 2 (b). It is obvious that the QT decomposition can adaptively control the block size of subdivision of image based on the region homogeneity. So QT decomposition can be used to determine the optimal subdivision of blocks. It is useful for eliminating the blocking artifacts of the fused image. In this paper, the maximum differences of the elements are used as the region homogeneity of the cartoon and texture components of the source images.

3 Multi-focus Image Fusion Based on Image Decomposition and QT Decomposition

3.1 Fusion Algorithm

In this section, a novel method based on image decomposition and QT decomposition is proposed. The proposed fusion framework is depicted in Fig. 3 and the detailed design is described as follows. For simplicity, this paper assumes that there are only two source images, namely I_A and I_B , here. The rationale behind the proposed scheme applies to the fusion of more than two multi-focus images. The source images are assumed to be pre-registered and the image registration is not included in the framework. The fusion algorithm consists of the following 3 steps:

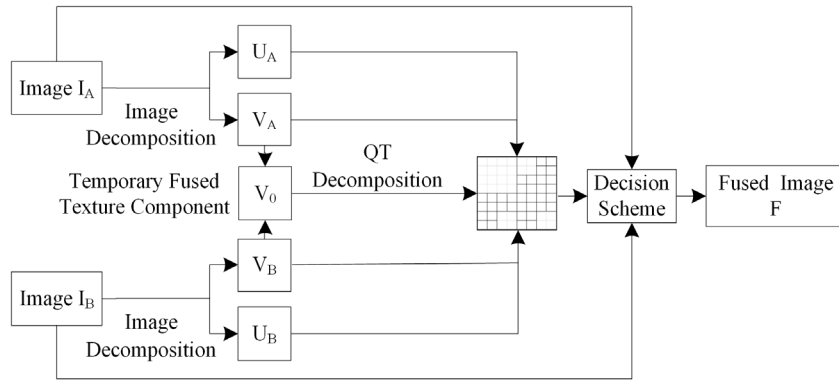


Fig. 3. Block diagram of proposed multi-focus images fusion framework.

Step 1: Perform the image decomposition on the source images I_A , I_B to obtain cartoon and texture components, respectively. The source image is decomposed as:

$$I = U + V . \quad (5)$$

For the source image I_A , let U_A , V_A denote the cartoon and texture components, respectively. For the source image I_B , U_B , V_B have the roles similar to U_A and V_A .

Step 2: Perform QT decomposition on the temporary fused component V_0 obtained by averaging V_A and V_B . U_A , U_B , V_A and V_B are partitioned based on the split result of the temporary fused component, respectively. To overcome the disadvantages of the small block in traditional block-based image fusion method, the minimum block size is set for terminating the further QT decomposition when the region homogeneity of the block doesn't meet the threshold condition. The region homogeneity is defined as:

$$|\max(V_{0(i,j)}^R) - \min(V_{0(i,j)}^R)| < T . \quad (6)$$

where $V_{0(i,j)}^R$ is the value of the pixel location (i, j) in temporary fused component V_0 . T is the threshold condition. In this paper, the threshold condition is set as 0.005 and the minimum block size is set as 8×8 .

Step 3: According to the fusion rules, the focused regions of the source images which corresponding to the focused regions of the cartoon and texture components are integrated to obtain the fused image F .

3.2 Fusion Rule

There are two key issues [25] for the fusion rules. One is how to measure the activity level of the cartoon and texture components, respectively, which recognizes the sharpness of the source images. Fig. 4 shows the relationship between the multi-component of the source images ‘Clock’ and their 3D shapes. It is obvious that the portion of the red circle in Fig. 4 (a) is more salient than the corresponding portion in Fig. 4 (b). The portion of the red circle in Fig. 4 (b) is more salient than the corresponding portion in Fig. 4 (a). The portion of the red circle in Fig. 4 (a) and Fig. 4 (b) are corresponding to the salient regions of the two cartoon components, respectively. Similarly, the portion of the red circle in Fig. 4 (c) is more salient than the corresponding portion in Fig. 4 (d). The portion of the red circle in Fig. 4 (d) is more salient than the corresponding portion in Fig. 4 (c). The portion of the red circle in Fig. 4 (c) and Fig. 4 (d) are corresponding to the salient regions of the two texture components, respectively. The salient regions of the cartoon and texture components are corresponding to the focused regions of the source images, respectively. Thus, we use the total EOG of each block of the cartoon and texture components to measure the activity level. The EOG of each block can be calculated as:

$$\begin{cases} EOG = \sum_i \sum_j (I_i^2 + I_j^2) \\ I_i = I(i+1, j) - I(i, j) \\ I_j = I(i, j+1) - I(i, j) \end{cases} \quad (7)$$

where $I(i, j)$ denotes the value of the pixel location (i, j) in the block of the cartoon or texture components.

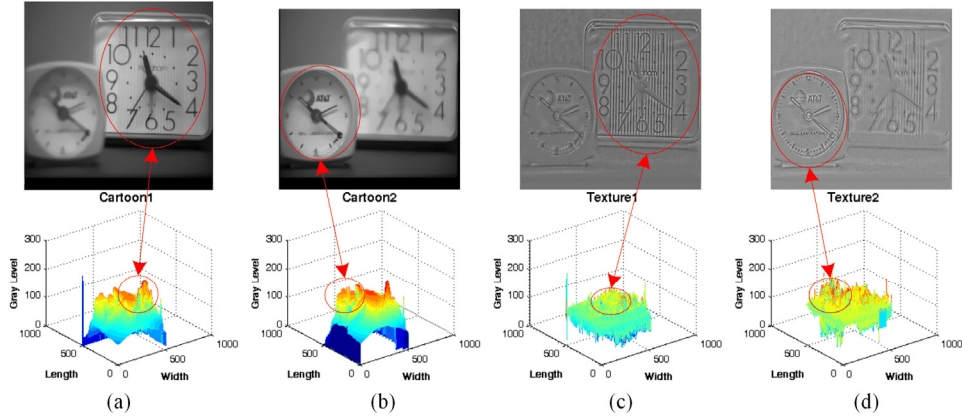


Fig. 4. The relationship between multi-component of the source images ‘Clock’ and their 3D shapes. (a) Cartoon component of the far focused image, (b) Cartoon component of the near focused image, (c) Texture component of the far focused image, (d) Texture component of the near focused image.

The other is how to integrate the focused pixels or regions of the source images which corresponding to the focused pixels or regions of the cartoon and texture components into the counterparts of the fused image. In order to eliminate the blocking artifacts, QT decomposition is applied to the cartoon and texture components. Let $U_A^{(k)}$ and $U_B^{(k)}$ denote the k th block of cartoon components U_A and U_B , respectively. Let $V_A^{(k)}$ and $V_B^{(k)}$ denote the k th block of texture components V_A and V_B , respectively. Let $EOG_k^{U_A}$ and $EOG_k^{U_B}$ denote the EOG of $U_A^{(k)}$ and $U_B^{(k)}$, respectively. Let $EOG_k^{V_A}$ and $EOG_k^{V_B}$ denote the EOG of $V_A^{(k)}$ and $V_B^{(k)}$, respectively. The total EOG of each block is calculated as:

$$\begin{cases} EOG_A = EOG_k^{U_A} + EOG_k^{V_A} \\ EOG_B = EOG_k^{U_B} + EOG_k^{V_B} \end{cases} \quad (8)$$

The total EOG of corresponding blocks are compared to determine which block is in focus. A decision matrix $H \in \mathbb{R}^{M \times N}$ is constructed for recording the comparison results according to the fusion rule as follows:

$$H(i, j) = \begin{cases} 1 & EOG_A \geq EOG_B \\ 0 & otherwise \end{cases} \quad (9)$$

where “1” in H indicates the pixel location (i, j) in image I_A is in focus while “0” in H indicates the pixel location (i, j) in image I_B is in focus.

$$F(i, j) = \begin{cases} I_A(i, j) & H(i, j) = 1 \\ I_B(i, j) & H(i, j) = 0 \end{cases} \quad (10)$$

However, judging by EOG alone is not sufficient to distinguish all the focused regions. There are thin protrusions, narrow breaks, thin gulfs, small holes, etc. in H . To overcome these disadvantages, morphological operations [26] are performed on H . Opening, denoted as $H \circ Z$, is simply erosion of H by the structure element Z , followed by dilation of the result by Z . This process can remove thin gulfs and thin protrusions. Closing, denoted as $H \bullet Z$, is dilation followed by erosion. It can join narrow breaks and thin gulfs. To correctly judge the small holes, a threshold is set to remove the holes smaller than the threshold. Thus, the final fused image F is constructed with Eq. (10). In this paper, the structure element Z of the proposed method is a 5×5 matrix with logical 1's and the threshold is set to 1000.

4 Experimental Results

In order to evaluate the performance of the proposed method, the experiment is performed on a set of 2 pairs of multi-focus source images [27] vary in content and texture, as shown in Fig. 5. The two pairs are all grayscale images with size of 640×480 pixels. In this paper, all the source images are assumed to have been registered. Experiments are conducted with Matlab in Windows environment on a computer with Intel Xeon X5570 and 48G memory. For comparison, besides the proposed method, some existing multi-focus image fusion methods are also implemented on the same set of source images. These existing methods include discrete wavelet transform (DWT), nonsubsampled contourlet transform (NSCT), SF (Li's method [4]), principal component analysis (PCA) and RPCA (Wan's method [10]). Due to the lack of original source code, the Eduardo Fernandez Canga's Matlab image fusion toolbox [28] is used as the reference for LAP, DWT, SF and PCA. Specifically, the Daubechies wavelet function 'bi97' is used in the DWT. The decomposition level of DWT is 4. The NSCT toolbox [29] is used as the reference for NSCT. The RPCA toolbox [30] is used as the reference for RPCA decomposition. The pyramid filter '9-7' and the orientation filter '7-9' with $\{4, 4, 3\}$ levels of decomposition are set for the fusion method based on NSCT. The Split Bregman toolbox [31] is used as the reference for the proposed method. In order to quantitatively compare the performance of proposed method and that of the others mentioned above, two metrics are used to evaluate the fusion performance. They are: (i) Mutual information (MI) [32], which measures the degree of dependence of the source images and the fused image. (ii) $Q^{AB/F}$ [33], which reflects the amount of edge information transferred from the source images to the fused image. A larger value for them means a better fusion result.

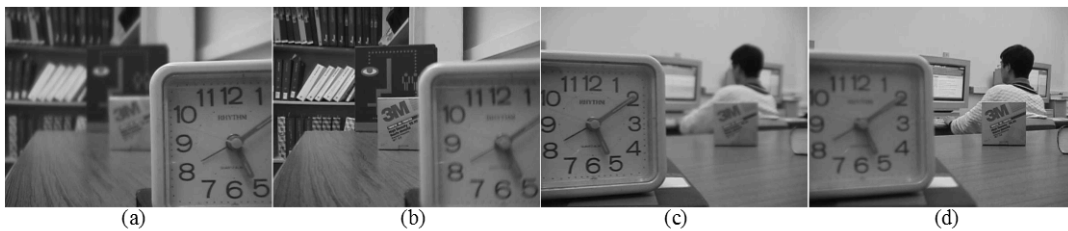


Fig. 5. Multi-focus source images. (a) Near focused image 'Disk', (b) Far focused image 'Disk', (c) Near focused image 'Lab', (d) Far focused image 'Lab'.

4.1 Qualitative Analysis

For qualitative comparison, the 'Disk' and 'Lab' fused images of different methods are shown in Fig. 6 and Fig. 7, respectively. The difference images between the far focused source image 'Lab' and its corresponding fused image obtained by different methods are shown in Fig. 8. Inspecting the book and the clock in Fig. 6, there are some obviously blurry regions between the white books and the bookcase in the fused images of DWT, NSCT and SF. Moreover, the obvious blocking artifacts appear on the upper edge of the clock in the fused image of SF. The left edge of the clock in the fused image of RPCA is incomplete. The contrast of the fused image of PCA is worse than that of the other methods. Inspecting the student and the clock in Fig. 7, the student's head in the fused images of DWT, NSCT shows obvious misregistration. The upper edge of the student's head of the fused image of RPCA has a narrow prominent. In Fig. 8, distortions are obviously observed in the difference images of DWT and NSCT. Mis-registration is also shown in the difference image of PCA. In addition, there are some obvious blocking artifacts in the difference image of SF. There are some obvious image residual in the right region of the difference image of RPCA. Thus, the fused image of proposed method achieves superior visual

performance by containing all the focused contents from the source images. But it should be noted that there are also some blocking artifacts in the edge of the clock in Fig. 6 (f). We attribute this to the fixed size of the structure element Z . To eliminate the thin protrusions, narrow breaks, thin gulfs, small holes, etc. in the decision matrix H , the morphological operations are performed on the decision matrix H by using the structure element Z with fixed size. The morphological operations lack adaptability for the fixed size of the structure element Z , which affects the fusion result. It cannot eliminate the thin protrusions, narrow breaks, thin gulfs, small holes, etc. in the decision matrix H completely.

4.2 Quantitative Analysis

For quantitative comparison, the quantitative results in two quality measures are shown in Table 1. The proposed method gains higher MI and $Q^{AB/F}$ values than the other methods. The running times are also shown in Table 1. One can see that the proposed method needs longer running time than the other methods except for NSCT and RPCA, due to the computation of total EOG of the cartoon and texture components of the source images accounts for the majority of the computational load.

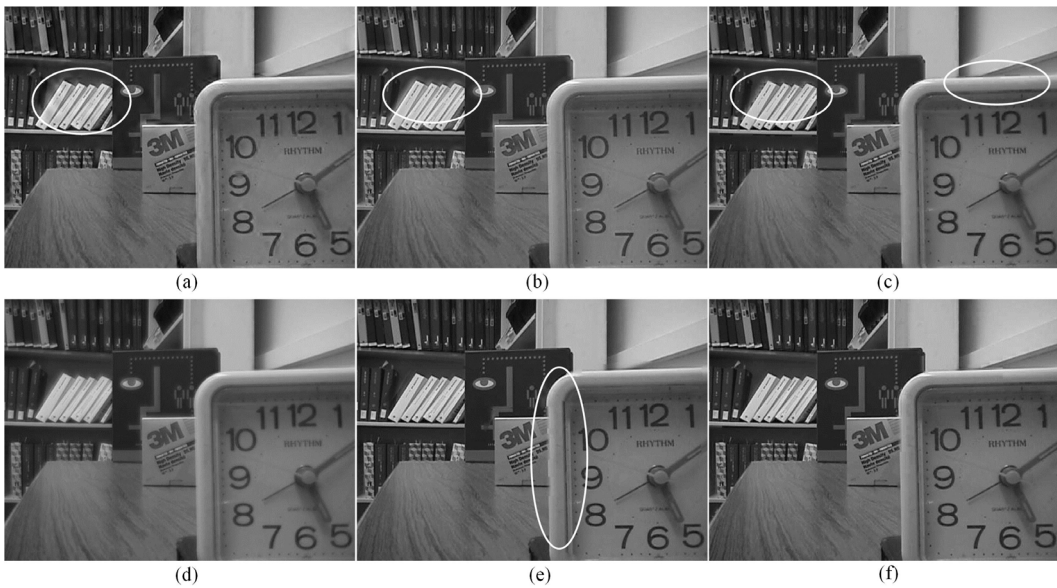


Fig. 6. The fused images ‘Disk’ obtained by DWT (a), NSCT (b), SF (c), PCA (d), RPCA (e), Proposed (f).

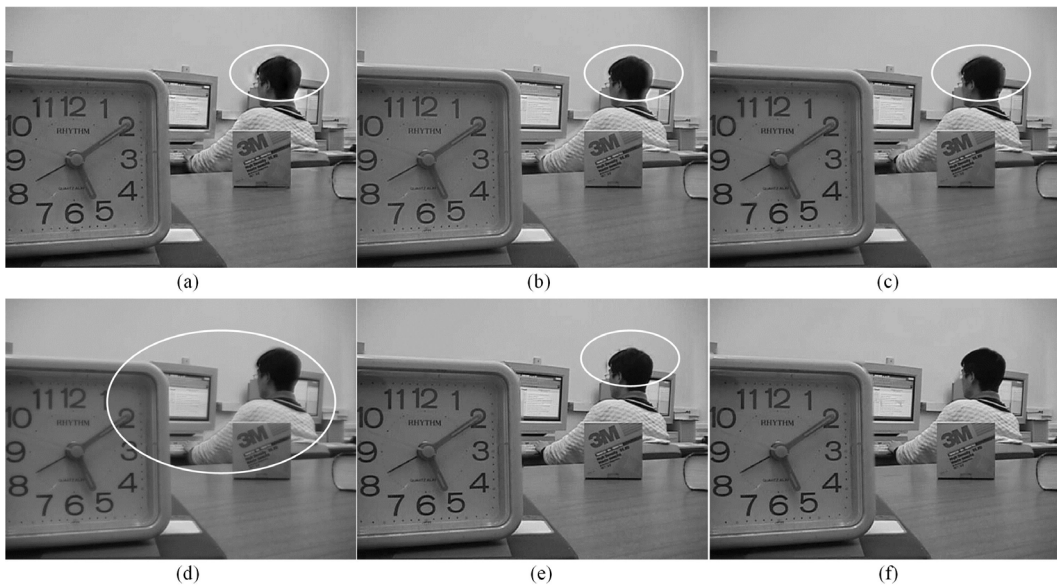


Fig. 7. The fused images ‘Lab’ obtained by DWT (a), NSCT (b), SF (c), PCA (d), RPCA (e), Proposed (f).

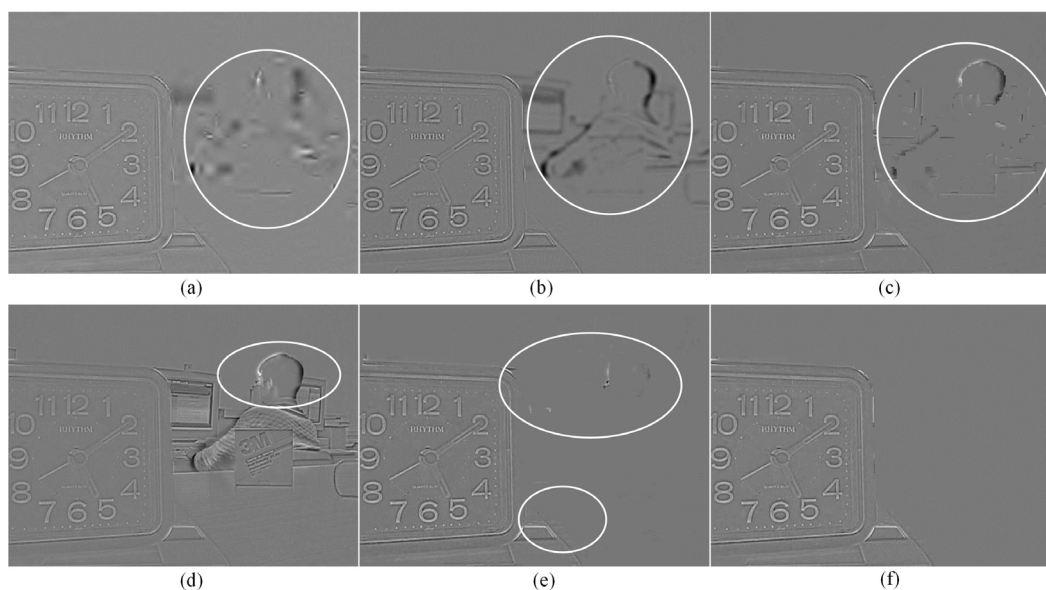


Fig. 8. The difference images between the right focused source image ‘Lab’ and the corresponding fused images obtained by DWT (a), NSCT (b), SF (c), PCA (d), RPCA (e), Proposed (f).

Table 1: The performance of different fusion methods for multi-focus image ‘Disk’ and ‘Lab’

Method	Disk			Lab		
	MI	$Q^{AB/F}$	Run-time (s)	MI	$Q^{AB/F}$	Run-time (s)
DWT	5.36	0.64	0.64	6.47	0.69	0.59
NSCT	5.88	0.67	463.20	6.95	0.71	468.51
SF	7.00	0.68	1.01	7.94	0.72	1.03
PCA	6.02	0.53	0.11	7.12	0.59	0.08
RPCA	8.12	0.72	60.38	8.50	0.75	60.80
Proposed	8.39	0.74	1.76	8.68	0.78	1.50

5 Conclusion and Future Work

In this paper, a novel multi-focus image fusion method is proposed to enhance the validity of focused regions extraction and blocking artifacts inhibition. The qualitative and quantitative evaluations have demonstrated that the proposed method can produce better fused image and significantly inhibit the blocking artifacts. But the proposed method is time-consuming for the computation of total EOG. In the future, we will consider optimizing the proposed method to reduce the computational cost and extending the developed method to the fusion of medical images.

Acknowledgement

The work is supported by the National Key Technology Science and Technique Support Program (No. 2013BAH49F03), the National Nature Science Foundation of China (No. 61379010), the Key Technologies R&D Program of Henan Province (No. 132102210515), the Natural Science Basic Research Plan in Shaanxi Province of China (No. 2012JQ1012).

References

- [1] G. Bhatnagar, Q. M. Jonathan Wu, Z. Liu, "Human Visual System Inspired Multi-Modal Medical Image Fusion Framework," *Expert Systems with Applications*, Vol. 40, pp. 1708-1720, 2013.
- [2] H. J. Zhao, Z. W. Shang, Y. Y. Tang, B. Fang, "Multi-focus Image Fusion Based on the Neighbor Distance," *Pattern Recognition*, Vol. 46, pp. 1002-1011, 2013.
- [3] S. T. Li, X. D. Kang, J. W. Hu, B. Yang, "Image Matting for Fusion of Multi-Focus Images in Dynamic Scenes," *Information Fusion*, Vol. 14, pp. 147-162, 2013.
- [4] S. T. Li, J. T. Kwok, Y. Wang, "Combination of Images with Diverse Focus Using Spatial Frequency," *Information Fusion*, Vol. 2, pp. 169-176, 2001.
- [5] W. Huang and Z. L. Jing, "Evaluation of Focus Measures in Multi-Focus Image Fusion," *Pattern Recognition Letters*, Vol. 28, pp. 493-500, 2007.
- [6] A. Goshtasby, "Fusion of Multi-Focus Images to Maximize Image Information," in *Proceedings of the 2006 Defense and Security Symposium*, pp. 17-21, 2006.
- [7] W. Huang and Z. L. Jing, "Multi-focus Image Fusion Using Pulse Coupled Neural Network," *Pattern Recognition Letters*, Vol. 28, pp. 1123-1132, 2007.
- [8] V. Aslantas and R. Kurban, "Fusion of Multi-focus Images Using Differential Evolution Algorithm," *Expert Systems with Applications*, Vol. 37, pp. 8861-8870, 2010.
- [9] I. De and B. Chanda, "Multi-focus Image Fusion Using a Morphology-Based Focus Measure in a Quad-tree Structure," *Information Fusion*, Vol. 14, pp. 136-146, 2013.
- [10] T. Wan, C. Zhub, Z. Qin, "Multifocus Image Fusion Based on Robust Principal Component Analysis," *Pattern Recognition Letters*, Vol. 34, pp. 1001-1008, 2013.
- [11] W. Casaca, A. Paiva, E. G. Nieto, P. Joia, L. G. Nonato, "Spectral Image Segmentation Using Image Decomposition and Inner Product-Based Metric," *Journal of Mathematical Imaging and Vision*, Vol. 45, pp. 227-238, 2013.
- [12] Y. F. Li and X. C. Feng, "Image Decomposition via Learning the Morphological Diversity," *Pattern Recognition Letters*, Vol. 33, pp. 111-120, 2012.
- [13] Z. C. Guo, J. X. Yin, Q. Liu, "On a Reaction-diffusion System Applied to Image Decomposition and Restoration," *Mathematical and computer modeling*, Vol. 53, pp. 1336-1350, 2011.
- [14] D. Mumford and J. Shah, "Optimal Approximations by Piecewise Smooth Functions and Associated Variational Problems," *Communications on Pure and Applied Mathematics*, Vol. 42, pp. 577-685, 1989.
- [15] L. Rudin, S. Osher, E. Fatemi, "Nonlinear Total Variation based Noise Removal Algorithms," *Physica D: Nonlinear Phenomena*, Vol. 60, pp. 259-268, 1992.
- [16] Y. Meyer, "Oscillating Patterns in Image Processing and Nonlinear Evolution Equations," *University Lecture Series*, AMS, pp. 22, 2001.
- [17] L. Vese and S. Osher, "Modeling Textures with Total Variation Minimization and Oscillating Patterns in Image Processing," *Journal of Scientific Computing*, Vol. 19, pp. 553-572, 2003.
- [18] S. Osher, A. Sole, L. Vese, "Image Decomposition and Restoration Using Total Variation Minimization and the H-1 Norm," *Journal of Scientific Computing*, Vol. 1, pp. 349-370, 2003.
- [19] J. F. Aujol and A. Chambolle, "Dual Norms and Image Decomposition Models," *International Journal of Computer Vision*, Vol. 63, pp. 85-104, 2005.

- [20] T. F. Chana, S. Esedoglua, F. E. Park, "Image Decomposition Combining Staircase Reduction and Texture Extraction," *Journal of Visual Communication and Image Representation*, Vol. 18, pp. 464-486, 2007.
- [21] T. Goldstein and S. Osher, "The Split Bregman Method for L1-Regularized Problems," *SIAM Journal on Imaging Sciences*, Vol. 2, pp. 323-343, 2009.
- [22] Y. L. Wang, J. F. Yang, W. T. Yin, Y. Zhang, "A New Alternating Minimization Algorithm for Total Variation Image Reconstruction," *SIAM Journal on Imaging Sciences*, Vol. 1, pp. 248-272, 2008.
- [23] S. Osher, M. Burger, D. Goldfarb, J. J. Xu, W. T. Yin, "An Iterative Regularization Method for Total Variation-Based Image Restoration," *Multiscale Modeling and Simulation*, Vol. 4, pp. 460-489, 2005.
- [24] P. Jagadeesh, P. Nagabhushan, R. P. Kumar, "A Novel Image Scrambling Technique Based On Information Entropy And Quad Tree Decomposition," *International Journal of Computer Science Issues*, Vol. 10, pp. 285-294, 2013.
- [25] Y. Jiang and M. H. Wang, "Image Fusion with Morphological Component Analysis," *Information Fusion*, Vol. 18, pp.107-118, 2014.
- [26] X. Z. Bai, F. G. Zhou, B. D. Xue, "Image Enhancement Using Multi-Scale Image Features Extracted by Top-Hat Transform," *Optics & Laser Technology*, Vol. 44, pp. 328-336, 2012.
- [27] Image sets: <http://www.ece.lehigh.edu/spcrl>, 2005.
- [28] Image fusion toolbox: <http://www.imagefusion.org/>.
- [29] NSCT toolbox: <http://www.ifp.illinois.edu/minhdo/software/>.
- [30] RPCA toolbox:http://perception.csl.illinois.edu/matrix-rank/sample_code.html.
- [31] Split Bregman toolbox: http://tag7.web.rice.edu/Split_Bregman_files/.
- [32] D. J. C. MacKay, "Information theory, inference and learning algorithms," *Cambridge university press*, 2003.
- [33] C. S. Xydeas and V. Petrovic, "Objective image fusion performance measure," *Electronics Letters*, Vol. 36, pp. 308-309, 2000.